JOURNAL OF PROPULSION AND POWER
Vol. 26, No. 4, July–August 2010

Particle Image Velocimetry Characterization of High-Speed Centrifugal Compressor Impeller-Diffuser Interaction

Kirk Gallier,* Patrick B. Lawless,† and Sanford Fleeter‡
Purdue University, West Lafayette, Indiana 47907

DOI: 10.2514/1.38663

High-density instantaneous and rotor phase-locked velocity field measurements are made in the centrifugal compressor diffuser vaneless space by means of the particle image velocimetry technique. The technique is challenged in this application by a small length scale and large velocities yielding very small flow time scales and demanding the use of extremely small flow tracking particles. The experiments reveal a detailed picture of the rotor phase-locked average impeller exit and diffuser inlet flowfield as is useful for unsteady flow modeling. Strong passage velocity gradients exist across the vaneless space up to the diffuser vanes, showing that the phase-locked averaged impeller exit flow presents a highly unsteady non-mixed-out velocity field for the downstream vane row. This unsteady vane intake is thus characterized by a strong fluctuation in incidence angle with the passing blade event. Measured time variation in the velocity field indicates a significant time-varying potential field due to incidence fluctuations.

Nomenclature

R_{duct}	=	inlet duct radius
r	=	radius
λ	=	radius ratio (diffuser leading-edge radius/impeller tip radius)
σ	=	1 standard deviation

I. Introduction

IMPELLER-DIFFUSER spacing is known to be an important parameter for design of centrifugal compressor vaned diffusers. Various centrifugal compressor literature sources [1–3] pose the importance of the vaneless space design for impact on performance parameters such as mass flow, operating range, stability limits, viscous loss, and diffuser separation to name a few. Several experimental studies have been conducted specifically on the affect of impeller-diffuser spacing and unsteady impeller-diffuser interaction. For example, Inoue and Cumpsty [4] reported point measurements of unsteady velocity and pressure in a low-speed centrifugal compressor with the aim of understanding impeller-diffuser interaction affects on diffuser performance. Arndt et al. [5,6] used a low-speed centrifugal pump to study the affect of the rotor pass event on unsteady loading of both the impeller and vane for several vane geometries. Their results provided useful relationship between specific geometry changes and decreases in unsteady blade loading.

A large number of reports have resulted from centrifugal compressor tests conducted at the DLR (German Aerospace Center) including several laser anemometry (L2F) investigations of the unsteady centrifugal compressor flow. These include an investigation by Domercq and Thomas [7] of unsteady velocity at three points within the vaneless space, but of most interest were their unsteady blade pressure measurements, which indicated strong fluctuations on the impeller blade surface and the vane suction surface in the semivaneless space region. Unsteady blade response measurements have also been reported by Jin et al. [8] for work on a moderate speed compressor, with testing several different diffuser inlet radius settings. The diffuser potential field was reported to have an impact on an unsteady separation in the impeller. These studies have reported specific component performance, component loading or vibration as being attributed to an impeller-diffuser interaction. However, little attention has been given to the details of the vaneless space unsteadiness as dependant directly upon the impeller-diffuser relative positioning. Additionally, most studies are limited to low-speed test facilities. Hathaway et al. [9] reported an effort to substantiate the use of a low-speed facility to validate a computational fluid dynamics model for high-speed compressor design and analysis. Their effort found that the secondary flow features of the impeller passage flow was highly dependent upon speed, indicating that the extension from low-speed testing to high-speed modeling is tenuous.

The current study is the first to include a high-speed experimental assessment of the full time variant vaneless space velocity field, and thus capture the detailed dynamics associated with impeller-diffuser interaction.

II. Technical Approach

The Purdue High-Speed Centrifugal Compressor designed by the Allison Engine Company (currently Rolls-Royce Company) is used for this work. The compressor consists of an advanced impeller design, a radial vaned diffuser, a discharge plenum and a bearing housing to support the compressor shaft. A layout of the compressor is shown in Fig. 1. The centrifugal impeller has a nominal operating speed of 48,450 rpm, a maximum pressure ratio of 5.4 and a maximum mass flow rate of 5.5 lb_m/s (2.5 kg/s). The design performance parameters of this compressor are listed in Table 1. Detailed descriptions of the overall facility layout and the specifics of available instrumentation are given in several references produced by past investigators [10–12]. Important to the current study is the diffuser to impeller spacing, which is given by the ratio of the diffuser inlet diameter to the impeller exit diameter, $\lambda = 1.094$.

A. Test Conditions

For the velocity measurements presented here, the compressor is operated near the 90% speed line. Specifically, the rotational rate is 43,300 rpm with a fluctuation of ± 30 rpm. The average test point is at a pressure ratio of 3.2404 ± 0.0213 and an inlet corrected mass flow rate of 4.1272 ± 0.0372 lb/s (1.872 kg/s), with both averaged

Presented as Paper 2007-5019 at the 43rd AIAA/ASME/SAE/ASEE Joint Propulsion Conference & Exhibit, Cincinnati, OH, 8–11 July 2007; received 20 May 2008; revision received 9 December 2009; accepted for publication 10 December 2009.

*Currently General Electric, 300 Garlington Road, Greenville, South Carolina 29615. Member AIAA.

†Currently Xcelaero Corp, 17230 Huffmeister Road Suite D, Cypress, Texas. Associate Fellow AIAA.

‡McAllister Distinguished Professor, Mechanical Engineering. Fellow AIAA.

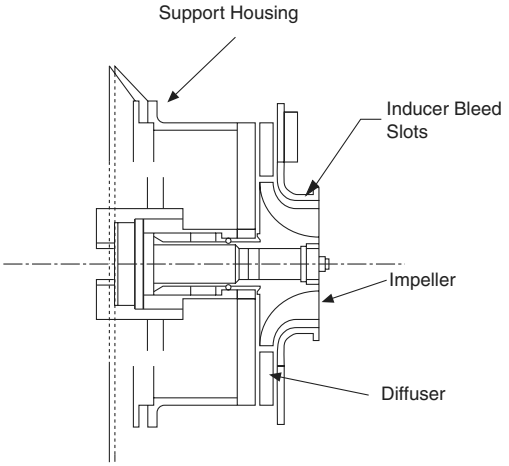

Fig. 1 High-speed centrifugal compressor.

values and the variation computed from 41 samples acquired during a continuous testing duration of over 9 h. This chosen test point is shown in Fig. 2, and is at a compressor speed line of interest due to proximity to a Campbell diagram frequency crossing. Thus, blade response measurements may be coupled with the current measurements.

Inlet conditions are captured from inlet total temperature and total pressure probes placed approximately 6 in. upstream of the impeller leading edge, within the inlet duct. Representative inlet conditions are given by an inlet static pressure of 8.2 psi (56 kPa), a total pressure profile of 8.67, 8.68, 8.67, and 8.57 psi (or 59.77, 59.85, 59.77, and 59.09 kPa) at radii, $r/R_{\text{duct}} = 0$, 0.54, 0.79, and 0.93, respectively. Likewise, the inlet total temperature is 81.5, 81.6, 81.3 F at radii, $r/R_{\text{duct}} = 0.5$, 0.71, and 0.86, respectively. The radius of the inlet duct is 2.85 in. (7.24 cm). The conditions are shown in Fig. 2.

B. Particle Image Velocimetry Measurement System

Velocity measurements are acquired in the diffuser vaneless space, between the impeller trailing edge and the diffuser vane leading edge. The measurement region, as shown in Fig. 3, spans a full vane pitch. The measurements are acquired using a Dantec Dynamics particle image velocimetry (PIV) system, a Hamamatsu C8484-05C digital camera, and a 50 mm Nikon macrolens.

The measurement system uncertainty is dependant upon displacement, distance, and time measures. Specifically, for velocities of 250 m/s, an optical scale factor of 36.32 pixels per millimeter, and a laser pulse delay time of 1000 ns, the imaged displacement for particles in the seeded flow is 9.1 pixels $\pm 1.1\%$. For a flow velocity of 450 m/s, particle displacements increase to an imaged displacement of 16.4 pixels $\pm 0.6\%$.

The imaged length scale is calibrated with a Max Levy #AA047 reticle calibration rule, which allows calibration of the target image over a length of 24 ± 0.001 mm. Because of optical grating the 24 mm calibration image distance is resolved to within ± 1 pixel, yielding an optical scale factor of 36.32 pixels per millimeter $\pm 0.11\%$.

Table 1 Geometry and performance parameters

Impeller	
Tip diameter, in. (cm)	8.520 (21.65)
Inlet Diameter, in. (cm)	5.6 (14.2)
Number of blades	15 w/splitters
Design speed, rpm	48,450
Max. pressure ratio	5.4
Max. flow rate, lb_m/s(kg/s)	5.5 (2.5)
Diffuser	
Inlet diameter, in. (cm)	9.320 (23.67)
Exit diameter, in. (cm)	13.6 (34.5)
Number of vanes	22
Axial passage width, in. (cm)	0.545 (1.3843)

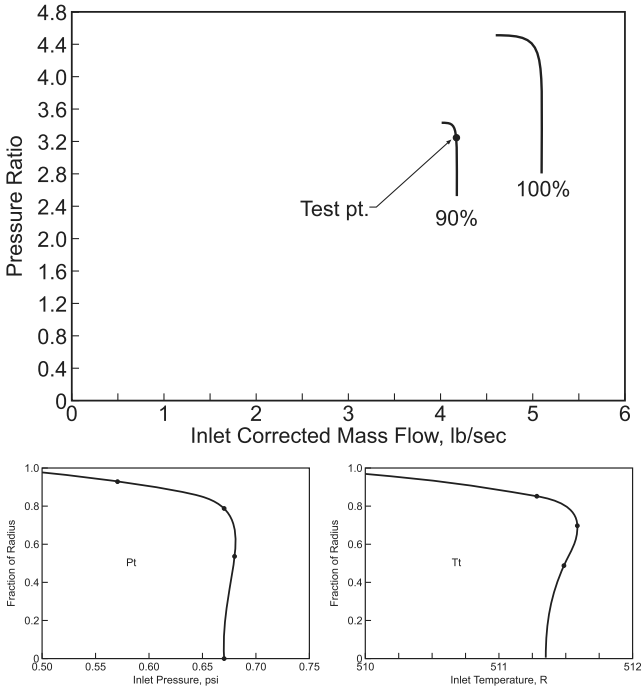

Fig. 2 Compressor characteristic and inlet conditions.

The pulsed laser time delay varies to no greater than $\pm 0.10\%$. Thus, the overall measurement uncertainty for the PIV system is dependant upon the actual flow velocities, and ranges from $\pm 1.11\%$ at the low end of velocity measured to 0.63% at the high end of measured velocities.

C. Flow Seeding

Nanometer sized particles introduced to the flow stream must accurately track the unsteady flow of interest. Various particle materials were evaluated analytically by assessment of each particle's aerodynamic response time based upon stokes drag in comparison to a flow time scale. This analysis is based upon a simplified Basset equation, and the work of Samimy and Lele [13]. The result is the choice of particle material DiEthyl Hexyl Sebacate (DEHS), which has a density of 912 kg/m^3, which is more than 4 times less the alternate solid particles of titanium dioxide.

These 0.25 μm DEHS particles can track 0.5 mm size flow structures with edge velocities of 450 m/s to within 1.09% of the true velocity [14]. These particles also have a high temperature capability and can be atomized with conventional means. An aerosol generator produced by Topas GmbH model ATM 210/H is modified with a larger liquid reservoir to handle extended operating times for this application.

D. Timing/Phase-Lock Averaging

Three hundred image pairs, i.e., flowfield samples, are acquired at each of 10 impeller positions for each of 6 axial measurement planes.

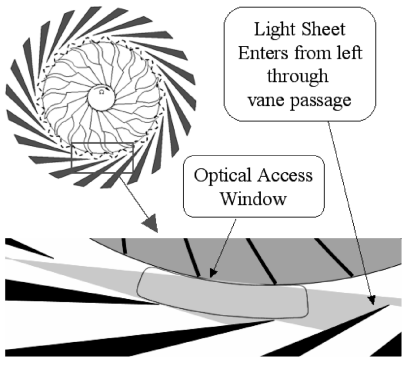

Fig. 3 Geometry and light sheet position.

Of the 10 impeller positions, each one represents an instant within the cycle of a single blade passing event. At each instance in this 10-position cycle, the 300 samples are averaged to present an average flowfield for that impeller position. These rotor phase-lock average flow fields are an average of a single blade pass as that unique blade passes by the sampling window 300 times.

III. Measurement Results

A presentation of measured velocities is made in terms of Mach number and flow angle. All Mach values are computed from the average velocity field and the mean computed acoustic speed of 411.786 m/s. Angle measurements are positive counter clockwise from tangential, forward looking aft.

Also, note that each vane has a 7.58 deg wedge angle, with the meanline angle of 10.35 deg, measured from tangential. The suction surface is at 6.56 deg from tangential and the pressure surface is at 14.14 deg from tangential. The zero incidence flow angle is taken to be 10.3 deg from tangential, where the radial direction is 90 deg from the tangential reference.

A. Relative and Absolute Frame Impeller Exit Profiles

Line plots of velocity in the rotating reference frame show the impeller exit flowfield, Fig. 4. This figure shows Mach number profiles at four constant radius offsets downstream of the impeller trailing edge at 35.3% span. The plot represents velocities for a single blade/vane relative position. A near uniform value of Mach number of approximately 0.3 exists from the suction side of the blade to 1/3 of the passage width. From that minimum Mach number to the pressure side of the blade a nearly constant gradient of Mach number exists. This profile indicates, that a low-momentum region like the wake of Dean's jet-wake model [15], exists near the suction side of the blade. The jet portion of that model is not accurately described by a uniform velocity profile in this case, as there is a nearly constant gradient of velocity from the wake fluid to the blade pressure surface. In that model, the shear layer between the jet and wake is ascribed as the source of rapid downstream mixing. In this case, the velocity measurements indicate a strong shear layer downstream of the blade trailing edge, which is anticipated to be the dominant mixing source.

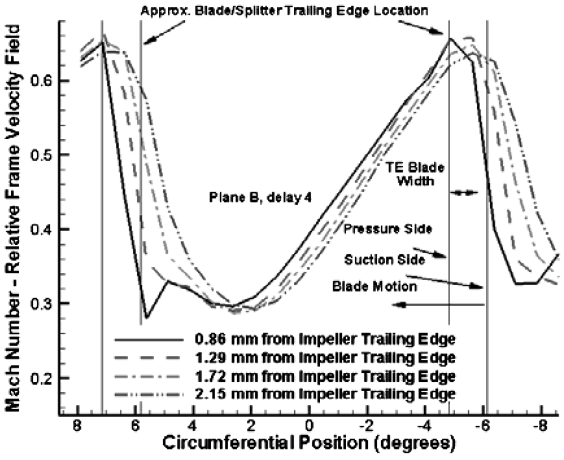

Fig. 4 Impeller trailing-edge relative frame Mach profile.

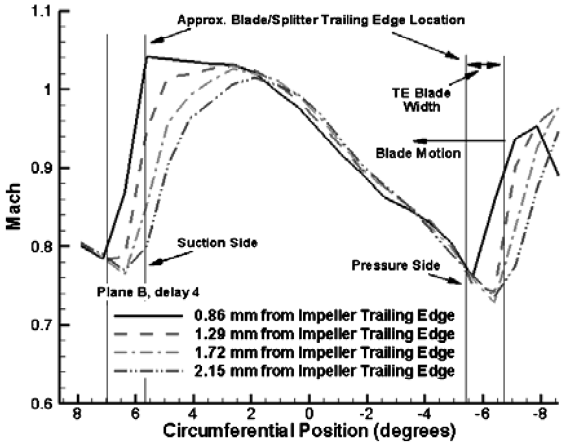

Fig. 5 Impeller TE absolute frame Mach profile.

While Fig. 4 is helpful for analogy to Dean's model, all below presentations of the Mach contours are presented in the absolute frame of reference. Thus, the same information as Fig. 4 is presented in Fig. 5 after coordinate transformation to the absolute frame. In a comparison of these two figures, it is clear that the low Mach value in the relative frame corresponds exactly to a high Mach number plateau in the absolute frame. And likewise, an increasing Mach number toward the pressure surface for the relative frame plot corresponds to a linearly decreasing Mach number toward the pressure surface for the absolute frame plot. An exceedingly sharp gradient in Mach number exists just downstream of the impeller blade for both of these cases, but with an opposite sign.

B. Full-Field Mach Contours

Three main features characterize the general flow, a high Mach zone, low Mach zone, and a diffuser vane leading-edge (LE) stagnation region, as shown in Fig. 6. The diffuser vane location is shown at the bottom of the image, and the measurement plane covers one full pitch of the diffuser passage. At the top of the image, the impeller blade trailing edge is shown with an accurately scaled blade thickness. The impeller blade motion in this representation is from right to left. The shown blade positioning is approximate with a possible error in positioning of 2% of a blade passage, which is due to small fluctuations in blade position at the time of measurement. The inaccuracy in position results from a signal acquisition time window for synchronization of the several PIV signal acquisition components.

The contour plot indicates that the impeller exit flow is characterized by a momentum gradient with high and low Mach regions also found in the above line plots. Additionally, a stagnation region or low-momentum region is shown near the leading edge of the diffuser vanes. All three of these flow components are dynamic and have a varying extent and intensity that depends upon both the relative blade-vane positioning as well as the axial position within the vaneless space.

Full-field velocity measurements are acquired at six planes spaced from the hub (aft) to the shroud (front) walls. Measurement planes A-F are at 23%, 35.3%, 45.7%, 56%, 66.4%, and 77% of the width of the vaneless space. For each of these planes 10 time instances are measured to capture the impeller-diffuser dynamic interactions. These 10 time instances correspond to 10 impeller positions, spaced equally through the duration of one blade passing period. In the following figures, these 10 instances are labeled in reference to an initial blade position and denoted by a time delay. The initial position and each successive impeller position are thus labeled as delay 0, delay 1, delay 2 and so on through delay 9. These 10 instances at each measurement plane are displayed in a clockwise sequence. Mach contours at 10 time instances are shown in Fig. 7.

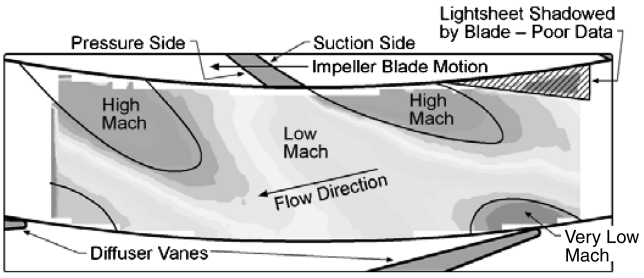

Fig. 6 General schematic of Mach field.

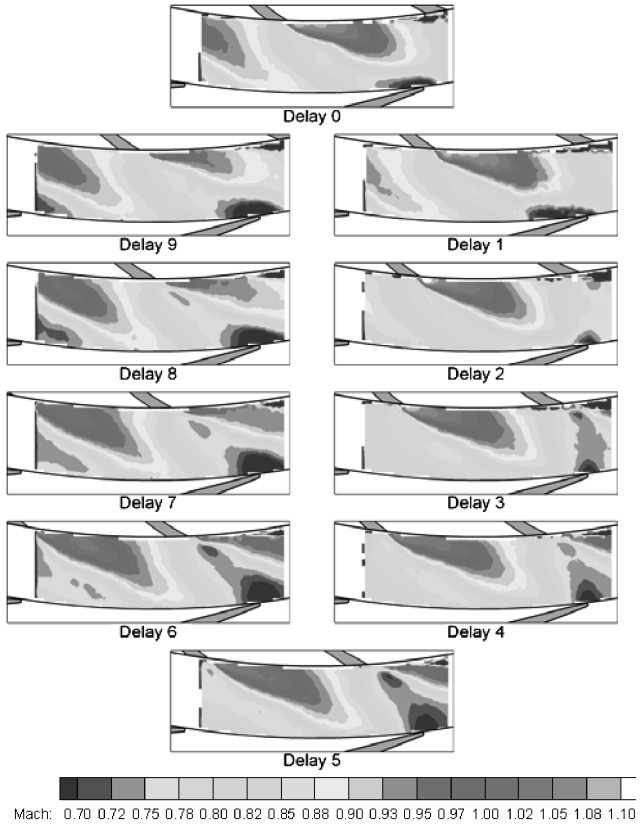

Fig. 7 Absolute frame Mach contours for 35.3% span at 10 impeller positions.

An interaction exists between the impeller exit flowfield and the diffuser. As the impeller passes by the diffuser, both the extent of the high Mach region is diminished by the presence of the vane, and the low Mach region is observed extending from the diffuser leading edge upstream to the impeller trailing edge.

First, the high Mach region at the impeller exit is modulated by the presence of the diffuser. This high Mach region continually increases after the blade passes the vane. Notice from delay frame 0 to frame 6 the extent of this high Mach region is gradually increasing. But, then from frame 6 to frame 9 there is a continual decrease in both radial extent and overall size of the same high Mach region. The presence of the diffuser vanes is the cause of this cyclic variation. The vane time mean potential field may be causing a slight blade-to-blade redistribution of mass flow in the impeller passage, realized in changes in the impeller exit flow rates during the impeller passing cycle. Additionally, the vaneless space flow is distributed such that there is a low flow region on the vane suction surface and higher flow rates toward the vane pressure surface. Again a vane-to-vane pressure field and a large positive time mean vane incidence angle, to be discussed later, are assessed as the cause of this flow distribution.

From Fig. 7 it appears that there is a difference in the flow downstream of the two neighboring impeller blades. The radial extent of the high Mach region appears deeper into the vaneless space for the lead blade than for the following blade. However, because only one passage from full blade-to-splitter blade passage is assessed through a cycle, and not two passages, it cannot be determined definitively that there is a larger wake region for the lead blade than the following blade. If differences are realized, they could be due to one being a full blade and its neighbor a splitter blade, each with different impeller passage flow.

Next consider the region of the low Mach number near the leading edge of the diffuser vane. In each of the 10 frames a low-momentum region persists at the leading edge of each diffuser vane. The extent of this low Mach region changes from confined to directly in front of the diffuser blade in frame 0 and frame 1 to extending fully from the diffuser leading edge radially inward to the impeller blade trailing edge in frames 2, 3, 4, and 5.

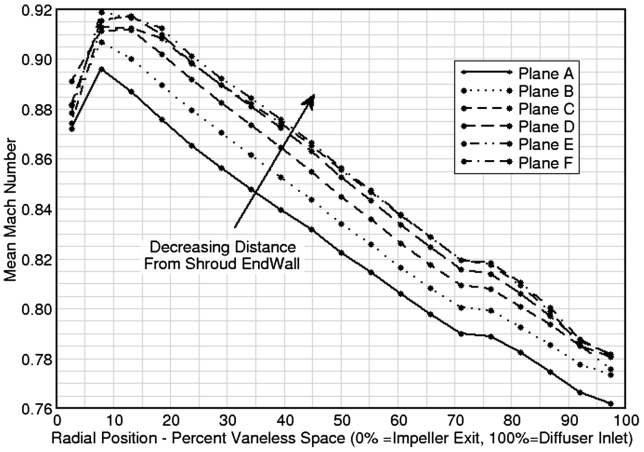

Fig. 8 Mean Mach number decay across vaneless space for six measurement planes.

Because by convection fluid is carried from right to left and diagonally downward from impeller exit plane toward the diffuser leading edge, this mean convection path would not account for the radial inward propagation of that low Mach region attached to the diffuser leading edge. Rather, this change in radial extent of the low Mach region, which happens as the blade passes the vane, is accounted for by an accompanying dynamic pressure field [14]. Additionally, notice in Fig. 7 that after a blade passes the diffuser leading edge, this low Mach region continues to be transported along the mean convection path. Finally this low-momentum fluid approaches the next vane leading edge further extending the low Mach region otherwise existing near the vane leading edge.

C. Time Mean Velocity

The time mean velocity variation in the vaneless space is approximately linear with radius, Fig. 8. This linear decrease with radius is to be expected. Because, by conservation of mass, the radial component of velocity will change inversely proportional to radius, and by conservation of angular momentum the tangential component of velocity will also change inversely proportional to radius, the linear decrease of absolute velocity is to be expected. The time mean profiles deviate from linear in two regions. First, over the initial 15% of the vaneless space there is an increase in Mach, which is attributed to both leakage effects at the hub wall gap (aft) and to a 5 deg pinch immediately downstream of the endwall gap. Such pinch or contraction is typically used for aiding flow stability in vaneless diffusers. Along the remaining distance to the vane LE, the vaneless space flow path has parallel planar end walls. And the deviation from

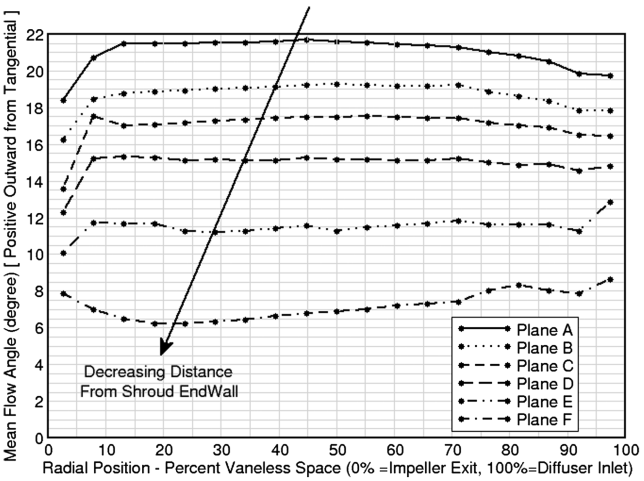

Fig. 9 Mean flow angle variation with radius.

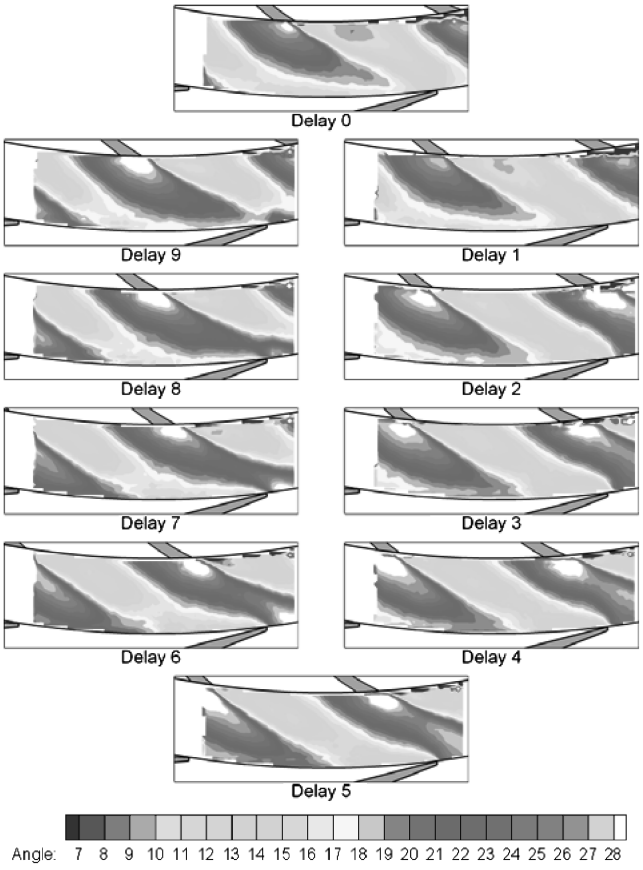

Fig. 10 Flow angle contours for plane B.

linear over the final 30% of the vaneless space is attributed to the vane potential field.

D. Flow Angle Variation

An unsteady vane potential field may be the cause of the time-varying Mach contours in Fig. 7. The cause of such a variation may be incidence driven.

First consider the time mean flow angle measurements. The time mean flow angle, plotted as a function of radial position in Fig. 9, shows a flow angle that is approximately constant with respect to the radial direction. The basic analytic model for the swirl of flow within a vaneless diffuser is a logarithmic spiral. This spiral is due to the radial component of velocity varying inversely to radius by conservation of mass, and the tangential component of velocity varying inversely to radius by conservation of angular momentum. The net result is a flow path where the angle between the tangential direction and the time mean streamline is a constant. This analytic model is consistent with the measured flow angles. Deviation from this description is only evident in close proximity to the impeller trailing edge and in close proximity to the diffuser vane leading edge.

However, whereas the measured time mean flow angle is consistent with the classic text book model of flow in a vaneless radial diffuser, the rotor phase-locked velocity measurements demonstrate a large circumferential gradient of flow angle at the impeller trailing edge, as well as a fluctuation of flowfield angles with rotor position. This fluctuation of flow angle with rotor position yields a strong variation in vane incidence. Table 2 summarizes the unsteady variation of the circumferential average flow angle at the measurement radius closest to the vane leading edge. The range of flow angles is given for each of the six spanwise measurement planes, and the fluctuation of the mean with rotor position. The Min Angle and Max Angle in the figure are the minimum and maximum circumferential averaged flow angles over the blade passing cycle.

The vaneless space flow angle variation with rotor position is further presented in Fig. 10. Generally, larger flow angles are found

Table 2 Vane LE flow angle variation with spanwise position

Position	% span	Min angle	Max angle	Mean incidence	Incidence variation (1σ)
A	23.0	13°	36°	9.4°	3.8°
B	35.3	11°	32°	7.6°	3.3°
C	45.7	10°	29°	6.2°	2.6°
D	56.0	9°	25°	4.5°	4.0°
E	66.4	7°	17°	2.4°	3.5°
F	77.0	4°	12°	−1.7°	4.7°

near the impeller blade pressure surface and smaller angles near the blade suction surface. These angles are due to the impeller exit profile. Also, larger flow angles are found near the vane pressure surface, and smaller flow angles near the vane suction surfaces. This is due to the flow response to the vane leading edge obstacle.

Consider the lower right hand vane leading edge approach flow in Fig. 10, from frame 8 to frame 9 to frame 0 there is a continual decrease in incoming flow angle. However, in frames 3–6 there is a continual and gradual increase in the angles in this region just upstream of the vane leading edge, so that over a large portion of the cycle the incidence angle is large, and it is clearly increasing in frame 4, 5, and 6 as the impeller blade approaches. After the impeller blade has passed, the incidence angle slowly reduces to its lowest values at frame 0 and 1. This cycle of variation in flow angle corresponds to the variation observed in the Mach number contours. The correspondence is in the fact that the cycle of incidence on the vane matches the cycle of variation in Mach number on the suction surface of the vane.

IV. Conclusions

The full-field velocity information depicts an impeller exit flowfield, which is characterized by a low-momentum wake, which spans from one third to nearly a full impeller passage. The remaining exit flowfield is shown in the ensemble average sense to be of a linear velocity gradient from this wake region to the facing blade pressure surface. This well-defined exit flowfield shows indication of differences from the full blade passage to the splitter passage, with one having a smaller wake region. This well-defined impeller exit flowfield is clearly defined deep into the vaneless space. The fact that strong velocity gradients exists up to the diffuser vane leading edge indicates that the average impeller exit flow presents a highly unsteady non-mixed-out velocity field for the downstream vane row. This unsteady vane intake is thus characterized by a strong fluctuation in incidence angle with the passing blade event.

From the impeller blade or relative frame perspective, the event of passing by the vane results in an increased impeller passage velocity gradient. The high positive flow angle associated with the strongly radial flow coming from the impeller pressure surface causes a large positive incidence on the diffuser vane. This positive incidence may momentarily increase vane loading, which would cause an increase in vane suction surface pressure in the semivaneless space, such an increased pressure would correspond with, in the absolute frame of reference, the measured increased low-momentum region. A higher pressure here would oppose the flow momentum, momentum that has a large circumferential component. This extended low-momentum region reaches fully to the impeller exit. And, what is a low-momentum region in the absolute frame is a high momentum region in the relative frame, that is to say that if a pressure wave propagated into the impeller pressure surface it would explain an increase in the relative frame velocities. These increased relative frame velocities correspond to an absolute frame flow with an increased radial component of momentum. This high radial momentum then translates to large flow angles and a large positive incidence presented to the next downstream vane, so that the cycle repeats.

This unsteady diffuser incidence may be a driver for both unsteady vane loading and unsteady impeller loading. This unsteady blade-vane interaction in the vaneless space is a potential participant in the problem of an impeller unsteady excitation.

Acknowledgment

This research was sponsored, in part, by the GUIde III Consortium on Blade Durability. This support is most gratefully acknowledged.

References

[1] Japikse, D., *Centrifugal Compressor Design and Performance*, Concepts ETI, Inc, Vermont, 1996.

[2] Krain, H., "Review of Centrifugal Compressor's Application and Development," *Journal of Turbomachinery*, Vol. 127, No. 1, Jan. 2005, pp. 26–34.

[3] Krain, H., "A Study on Centrifugal Impeller and Diffuser Flow," *Journal of Engineering for Power*, Vol. 103, No. 4, 1981, pp. 688–697.

[4] Inoue, M., and Cumpsty, N. A., "Experimental Study of Centrifugal Impeller Discharge Flow in Vaneless and Vaned Diffusers," *Journal of Engineering for Gas Turbines and Power*, Vol. 106, 1984, pp. 455–467.

[5] Arndt, N., Acosta, A. J., Brennen, C. E., and Caughey, T. K., "Rotor-Stator Interaction in a Diffuser Pump," *Journal of Turbomachinery*, Vol. 111, No. 3, 1989, pp. 213–221. doi:10.1115/1.3262258

[6] Arndt, N., Acosta, A. J., Brennen, C. E., and Caughey, T. K., "Experimental Investigation of Rotor-Stator Interaction in a Centrifugal Pump with Several Vaned Diffusers," *Journal of Turbomachinery*, Vol. 112, No. 1, 1990, pp. 98–108. doi:10.1115/1.2927428

[7] Domercq, O., and Thomas, R., "Unsteady Flow Investigation in a Transonic Centrifugal Compressor," AIAA Paper 97-2877, 1997.

[8] Jin, D., Jiang, Z., Hasemann, H., Haupt, U., and Rautenberg, M., "Influence of Vaned Diffuser on Dangerous Blade Vibration Due to Blade flow Interactions in a Centrifugal Compressor," American Society of Mechanical Engineers Paper 95-GT-122, 1995.

[9] Hathaway, M. D., Chriss, R. M., Wood, J. R., and Strazisar, A. J., "Experimental and Computational Investigation of the NASA Low-Speed Centrifugal Compressor Flow Field," *Journal of Turbomachinery*, Vol. 115, 1993, pp. 527–542.

[10] Shook, Patrick, "The Aerodynamic Performance of a High Speed Research Centrifugal Compressor," M.S. Thesis, Mechanical Engineering Dept., Purdue Univ., 1994.

[11] Oakes, William, "Characterization of Instability Initiation in Centrifugal Compressors," Ph.D. Dissertation, Mechanical Engineering Dept., Purdue University, 1997.

[12] Carnell, W. F., Jr., "Aerodynamic Performance and Forcing Function Measurements in a High-Speed Centrifugal Compressor," M.S. Thesis, Mechanical Engineering Dept., Purdue Univ., 2002.

[13] Samimy, M., and Lele, S. K., "Motion of Particles with Inertia in a Compressible Free Shear Layer," *Physics of Fluids*, Vol. 3, 1991.

[14] Gallier, K. D., "Experimental Characterization of High Speed Centrifugal Compressor Aerodynamic Forcing Functions," Ph.D. Dissertation, Mechanical Engineering Dept., Purdue Univ., 2005.

[15] Dean, R. C., "The Fluid Dynamic Design of Advanced Centrifugal Compressors," Lecture Notes Presented at the Von Karman Institute, March 1974.

C. Tan
Associate Editor